https://doi.org/10.5194/essd-2021-443
Preprint. Discussion started: 3 February 2022

Earth System Science Data
Open Access Discussions

New gridded dataset of rainfall erosivity (1950–2020) on the Tibetan Plateau

Yueli Chen[1], Xingwu Duan[2], Minghu Ding[1], Wei Qi[1], Ting Wei[1], Jianduo Li[3]

[1]Institute of Tibetan Plateau and Polar Meteorology, Chinese Academy of Meteorological Sciences, Beijing, 100081, China
[2]Institute of International Rivers and Eco-security, Yunnan University, Kunming, 650091, China
[3]China Meteorological Administration Earth System Modeling and Prediction Centre, Beijing, 100081, China

Correspondence to: Xingwu Duan (xwduan@ynu.edu.cn), Minghu Ding (dingminghu@foxmail.com)

Abstract. The risk of water erosion on the Tibetan Plateau (TP), a typical fragile ecological area, is increasing with climate change. Rainfall erosivity maps are useful for understanding the spatiotemporal patterns of rainfall erosivity and identifying vulnerable regions. This study generated a gridded annual rainfall erosivity dataset of the TP for 1950–2020 using a new approach based on 1-min precipitation observations at 1787 weather stations and 0.25° hourly European Center for Medium-Range Weather Forecasts Reanalysis 5 (ERA5) precipitation data. We conclude that ERA5 is generally useful for mapping annual rainfall erosivity on the TP, considering the high correlation coefficient and consistent spatiotemporal patterns between the ERA5-based and observed annual rainfall erosivity. In addition, obvious underestimation of the ERA5-based annual rainfall erosivity was found. After correction by a multiplier factor map, the annual rainfall erosivity values for 2013–2020 are in good agreement with the observed values in terms of the correction coefficient and probability density. Finally, a new annual rainfall erosivity dataset for 1950–2020 was produced after the ERA5-based annual rainfall erosivity values were corrected. We found that the area-averaged mean annual rainfall erosivity on the TP is 307 $MJ \cdot mm \cdot ha^{-1} \cdot h^{-1}$ and tends to decrease from southeast to northwest. Key regions with large rainfall erosivity potential are concentrated in the Bomi–West Sichuan and Dawang–Chayu areas. This new annual rainfall erosivity dataset could extend our knowledge of rainfall erosivity patterns and provide fundamental data for quantifying soil erosion in the TP.

https://doi.org/10.5194/essd-2021-443
Preprint. Discussion started: 3 February 2022

1 Introduction

Precipitation is the main driver of water erosion because it directly affects the detachment of soil particles, breakdown of aggregates, and transport of eroded particles via runoff (Wischmeier and Smith, 1965, 1978). The *R* factor, that is, the multi-year average rainfall erosivity, which is described by the Uiversal Soil Loss Equation (USLE; Wischmeier and Smith, 1965, 1978) and Revised USLE (Renard, 1997), is an indicator of the multi-year average potential ability of rainfall and runoff to affect soil erosion. The *R* factor is calculated using the classical (Wischmeier and Smith, 1965) and statistical algorithms (e.g., Liu et al., 2002) according to the temporal resolution of the precipitation data.

The classical algorithm for rainfall erosivity requires a continuous precipitation data series with <15-min temporal resolution (Angulo-Martínez and Beguería, 2009). As networks of weather stations and observation platforms have matured considerably in the past two decades, rainfall erosivity has been calculated using the classical algorithm at the local scale (Agnese et al., 2006; Ma et al., 2014; Wang et al., 2017), and the application of the algorithm has been gradually extended to the national (Panagos et al., 2015; Kim et al., 2020; Yue et al., 2021) and global scale (Panagos et al., 2017; Liu et al., 2020). Despite substantial progress, it is still notable that the relative error of the estimated rainfall erosivity increases rapidly with increasing time interval of the precipitation data. For example, the relative error based on hourly data was more than 80%, compared with the results based on 1-min data (Lobo and Bonilla, 2015; Yin et al., 2015; Shin et al., 2019). In addition, the accuracy of the rainfall erosivity is greatly reduced by inadequate weather station coverage, especially in areas with complex climates and terrains (Yue et al., 2021). Therefore, the accuracy of rainfall erosivity estimation depends strongly on the temporal and spatial resolution of the precipitation observations (Panagos et al., 2017; Kim et al., 2020).

Compared with station-based observations, gridded precipitation data from radar-based and satellite-based datasets cover larger areas for longer periods. These gridded data have been widely used to estimate the rainfall erosivity in China (Teng et al., 2018), Germany (Risal et al., 2018), Africa (Vrieling et al., 2010), the United States (Kim et al., 2020), and other regions. They have contributed greatly to our knowledge of the spatiotemporal patterns of rainfall erosivity; however, the uncertainties in rainfall erosivity obtained using gridded data have not been quantified, although obvious biases between gridded and observed precipitation values have been demonstrated (Freitas et al., 2020).

https://doi.org/10.5194/essd-2021-443
Preprint. Discussion started: 3 February 2022

The Tibetan Plateau (TP) referred to as the Third Pole is one of the highest plateaus worldwide and has an average altitude of more than 4000 m (Yao et al., 2012). Since the mid-1950s, the TP has experienced significant warming exceeding that of other regions in the same latitude zone (Liu and Chen, 2000). Owing to increasing snowmelt and more frequent heavy precipitation events, which may cause more severe soil erosion, knowledge of the rainfall erosivity on the TP is highly important for soil sustainability and thus water and food security. The accuracy of rainfall erosivity estimation depends mainly on the spatiotemporal accuracy of the precipitation data, especially in the TP, where the seasonal and regional precipitation patterns exhibit significant variability owing to westerly winds, the Indian monsoon, and land–atmosphere interaction.

Many efforts have been made to study rainfall erosivity on the TP. Most studies have used precipitation observations from dozens of weather stations with inadequate time span (e.g., Gu et al., 2020), yet it is difficult to accurately obtain the long-term rainfall erosivity on the TP. In particular, considering the complex precipitation patterns over the TP, there are large uncertainties in the rainfall erosivity obtained by the interpolation of scarce in-situ values, which greatly limit our understanding of the spatiotemporal patterns of rainfall erosivity. Over the past decade, the application of gridded precipitation datasets has expanded the spatiotemporal scale of studies of rainfall erosivity on the TP (e.g., Cao et al., 2018). However, the bias of gridded precipitation data has been found to vary depending on the region, and the calculation biases resulting from the use of gridded data have not yet been extensively evaluated and corrected. Thus, the rainfall erosivity, that is, the *R* factor, strongly affects the accuracy of soil erosion estimation on the TP.

The main objective of this study is to generate a long-term, high-precision annual rainfall erosivity dataset that combines the advantages of station-based observations and gridded data. The multi-source precipitation datasets, including the 1-min precipitation observations at 1787 weather stations for 8 years and 0.25° hourly European Center for Medium-Range Weather Forecasts (ECMWF) Reanalysis 5 (ERA5) data for 71 years, are used. This paper describes (1) the assessment of the ERA5 data for estimating rainfall erosivity on the TP; (2) the correction of the ERA5-based annual rainfall erosivity and validation of the corrected values; and (3) the generation of an annual rainfall erosivity dataset with 0.25° resolution for 1950–2020.

2 Study Area and Source Data

https://doi.org/10.5194/essd-2021-443
Preprint. Discussion started: 3 February 2022

2.1 Tibetan Plateau

The study area is the TP (26–40°N, 73–105°E), which is located in Southwestern China and covers an area of approximately 2.5 million km^2. The elevation of the TP ranges from 84 to 8246 m, with an average value of 4379 m. Precipitation in the southeastern TP is influenced by warm, humid Indian monsoons, whereas in the western TP, it is influenced more strongly by the mid-latitude westerlies (Yao et al., 2012). The annual precipitation is concentrated from May to October (Gu et al., 2020), and shows a spatial pattern of a wet east and west with a dry middle (Li et al., 2020). Along with the significant climate change and a very fragile ecological environment, the TP has high potential for soil loss, especially in the eastern TP and Hengduan Mountains, which are among the most severely eroded areas in China (Teng et al., 2019).

2.2 Precipitation data

Previous studies of the TP have used in-situ precipitation observations with <50 stations and coarse temporal resolution, e.g., hourly (Yue et al., 2021), daily (Wang et al., 2017), or half-monthly (Teng et al., 2018; Gu et al., 2020; Liu et al., 2020). By contrast, this study estimated the rainfall erosivity on the TP using precipitation observations at 1-min intervals in 2013–2020 at 1787 weather stations obtained from the National Meteorology Information Center of the China Meteorological Administration [Figure 1(a)].

To ensure the accuracy of the in situ precipitation data, we evaluated their quality. The data integrity of each station was first checked using quality control codes at 1-min intervals by month. Because precipitation on the TP occurs mainly from May to September, observed data with an integrity of >90% from May to September in a year can be used to calculate the annual rainfall at the station. The number of stations with data suitable for calculating the annual rainfall erosivity for each year is shown in the lower left corner of Figure 1(a); it ranges from 628 to 1472, with an average of 1114 stations for 2013–2020 (excluding 2017, because a disruption in data reception caused the loss of precipitation observations in August 2017). Moreover, we examined the station density in each 0.25° grid, which is consistent with the spatial resolution of the ERA5 data [Figure 1(b)]. The number of stations in each grid varies from 1 to 29, and the mean value is 2.1. A total of 836 grids (20% of the grids covering the TP) have observed precipitation values. Because the data quality varies, the available grids with

https://doi.org/10.5194/essd-2021-443
Preprint. Discussion started: 3 February 2022

observations change annually; on average, there are 589 available grids with observation records for 2013–2020, excluding 2017.

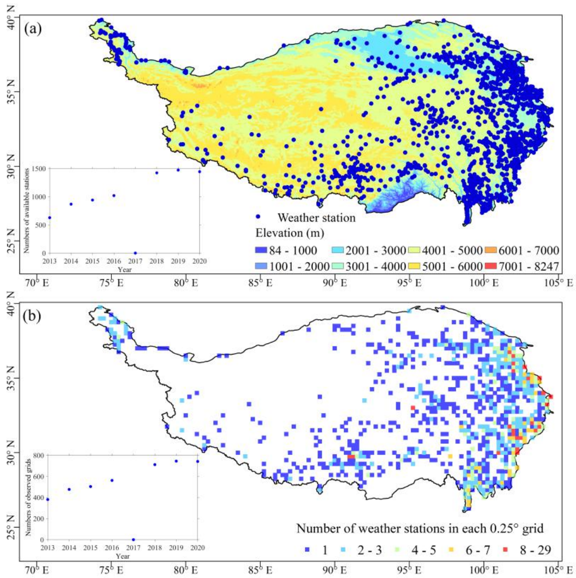

Figure 1. (a) Spatial distribution of weather stations on TP; the inset shows the number of available weather stations by year. (b) Number of available weather stations in each grid with 0.25° spatial resolution; the inset shows the number of available weather stations by year.

The hourly 0.25° ERA5 data represent the most recent generation of ECMWF global atmospheric reanalysis and offer higher spatial resolution than ERA-Interim and other improvements since 1979 (Hersbach et al., 2019). The precipitation data are the sum of large-scale precipitation and convective precipitation consisting of rain and snow, as determined by the ECMWF Integrated Forecasting System.

3 Methodology

To reconstruct the annual rainfall erosivity on the TP for 1950–2020, 1-min precipitation observations and 0.25° hourly ERA5 gridded precipitation data were used. Figure 2 shows the algorithm for generating the annual rainfall erosivity. For this purpose, we first divided the station-based grid values of the annual rainfall erosivity by the ERA5-based values to obtain the multiplier factor. Next, a multiplier factor map of the TP was generated using inverse distance weighted (IDW) interpolation. The obtained ERA5-based annual rainfall erosivity map was corrected by the multiplier factors for 1950–2020, and the accuracy of the corrected annual rainfall erosivity maps for 2013–2020, excluding 2017, was evaluated.

https://doi.org/10.5194/essd-2021-443
Preprint. Discussion started: 3 February 2022

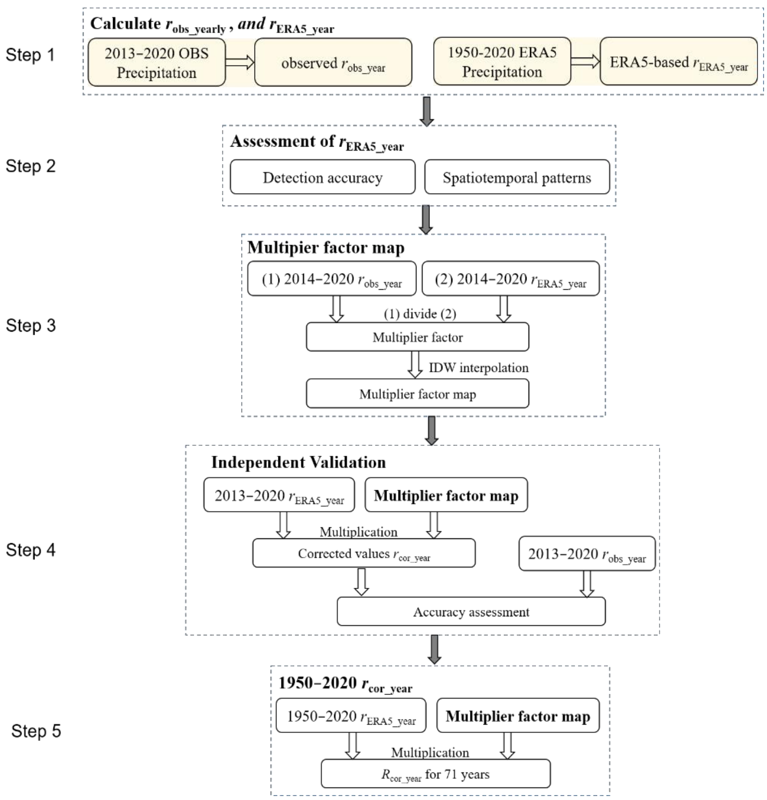

Figure 2. Schematic representation of algorithm for generating annual rainfall erosivity dataset for 1950–2020.

3.1 Algorithm of annual rainfall erosivity

A rainfall event is defined following Wischmeier and Smith (1978) as having measurable rainfall with no interruption or at most a 6-h interruption. If a rainfall event is interrupted for more than 6 h, subsequent rainfall is considered to belong to a new rainfall event. Rainfall events of more than 12 mm are selected as erosive events following Xie et al. (2000), and the EI_{30} index of the erosive event is calculated. Specifically, the rainfall erosivity of an erosive rainfall event is calculated as follows (Brown and Foster, 1987):

$$e_r = 0.29[1 - 0.72\exp(-0.05 i_r)] \quad (1)$$

$$E = \sum_{r=1}^{n} (e_r \cdot P_r) \quad (2)$$

$$r_{event} = E \cdot I_{30} \quad (3)$$

where E (MJ·ha^{-1}) is the total energy of the erosive event, and r_{event} (MJ·mm·ha^{-1}·h^{-1}) is the event rainfall erosivity of the event. For the 1-min precipitation data (ERA5 data), i_r (mm/h) is the rainfall

https://doi.org/10.5194/essd-2021-443
Preprint. Discussion started: 3 February 2022

intensity for the r^{th} minute (hour), e_r (MJ·ha^{-1}·mm^{-1}) is the unit energy for the r^{th} minute (hour), P_r (mm) is the rainfall amount for the r^{th} minute (hour), n is the rainfall duration, and I_{30} (mm/h) is the maximum contiguous 30-min (1-h) peak intensity. After the event rainfall erosivity at all stations was calculated, we identified and removed extreme outliers of the event rainfall erosivity at each site, which resulted from temporary abnormalities in the automatic observation equipment and were not identified during quality control of the precipitation data. We used boxplots to detect extreme outliers. The lower and upper quartiles were defined as the 25th percentile of event rainfall erosivity (Q1) and the 75th percentile (Q2); the difference (Q2 − Q1) is called the interquartile range (IQR). Event rainfall erosivity data at a station outside the lower and upper bounds (Q1 − 3IQR, Q2 + 3IQR) are considered extreme outliers.

The observed annual rainfall erosivity values ($r_{\text{station\_year}}$) were obtained by summing the rainfall erosivity for all erosive events per year by station. Next, the ERA5-based annual rainfall erosivity ($r_{\text{ERA5\_year}}$) for all the grids in the TP were calculated. Notably, for easy comparison of $r_{\text{station\_year}}$ and $r_{\text{ERA5\_year}}$, the $r_{\text{station\_year}}$ values were upscaled to the grid values ($r_{\text{obs\_year}}$) with 0.25° spatial resolution by averaging the station-based values in the same grid. Figure 1(b) shows the spatial distribution of the available grids with $r_{\text{obs\_year}}$. Steps 2 to 5 in Figure 2 are all based on $r_{\text{obs\_year}}$ and $r_{\text{ERA5\_year}}$ data.

3.2 Assessment of ERA5-based annual rainfall erosivity estimation

The mean values of $r_{\text{ERA5\_year}}$ for 2013–2020 were compared with those of $r_{\text{obs\_year}}$ by station. The absolute bias (AB) and correction coefficient (r) were used to evaluate the accuracy of annual rainfall erosivity estimation using ERA5 data. The AB is calculated as shown in Eq. 4.

$$AB = \sum_{i=1}^{n} \left(r_{\text{ERA5\_year}_i} - r_{\text{obs\_year}_i}\right) / n \qquad (4)$$

where i is the i^{th} annual rainfall erosivity value, $r_{\text{ERA5\_year}_i}$ is the ERA5-based annual rainfall erosivity in the i^{th} year, $r_{\text{obs\_year}_i}$ is the observed annual rainfall erosivity in the i^{th} year, and n is the number of years of data. Moreover, the empirical orthogonal function (EOF) was employed to assess the spatiotemporal pattern of annual rainfall erosivity revealed by the ERA5 reanalysis precipitation data by comparing it with the pattern revealed by the observed values.

3.3 Reconstruction and validation of annual rainfall erosivity

The results presented in section 4.1 show a high correlation between the observed and ERA5-based

https://doi.org/10.5194/essd-2021-443
Preprint. Discussion started: 3 February 2022

annual rainfall erosivity in 2013–2020, and their spatiotemporal distribution patterns show reasonable agreement. Consequently, the long-term dataset of annual rainfall erosivity can be obtained by correcting the ERA5-based values. We used a multiplier factor method to improve the accuracy of the ERA5-based annual rainfall erosivity; this method is commonly used to correct precipitation amounts (He et al., 2020). First, the $r_{\mathrm{obs\_year}}$ values were divided by $r_{\mathrm{ERA5\_year}}$ for each year, and then the calculated results, i.e., the multiplier factor values, were averaged for each year. Second, IDW interpolation was used to generate a multiplier factor map of the TP with 0.25° spatial resolution. Finally, the corrected annual rainfall erosivity dataset ($r_{\mathrm{cor\_year}}$) was obtained as the product of $r_{\mathrm{ERA5\_year}}$ and the multiplier factor for each grid.

Specifically, there are 373 grids with observed annual rainfall erosivity values from 2014 to 2020. The $r_{\mathrm{obs\_year}}$ and $r_{\mathrm{ERA5\_year}}$ values in these grids were used to generate the multiplier factor map. The $r_{\mathrm{obs\_year}}$ and $r_{\mathrm{ERA5\_year}}$ values in other grids for 2014–2020, which were not used, are available for assessing the accuracy. Moreover, all of the data for 2013 were treated as an independent set for verification; in other words, none of these data were used to generate the multiplier factor map. Table 1 lists the number of validation grids for each year, and Figure 3 shows the spatial distribution of the validation grids for 2013–2020 (excluding 2017).

Table 1. Numbers of grids used in this study

Year	Total number of grids with observations	Number of validation grids	Percentage of validation data in total data (%)
2013	***381***	***381***	***100***
2014	477	104	22
2015	504	131	26
2016	562	189	34
2018	712	339	48
2019	745	372	50
2020	742	369	50

https://doi.org/10.5194/essd-2021-443
Preprint. Discussion started: 3 February 2022

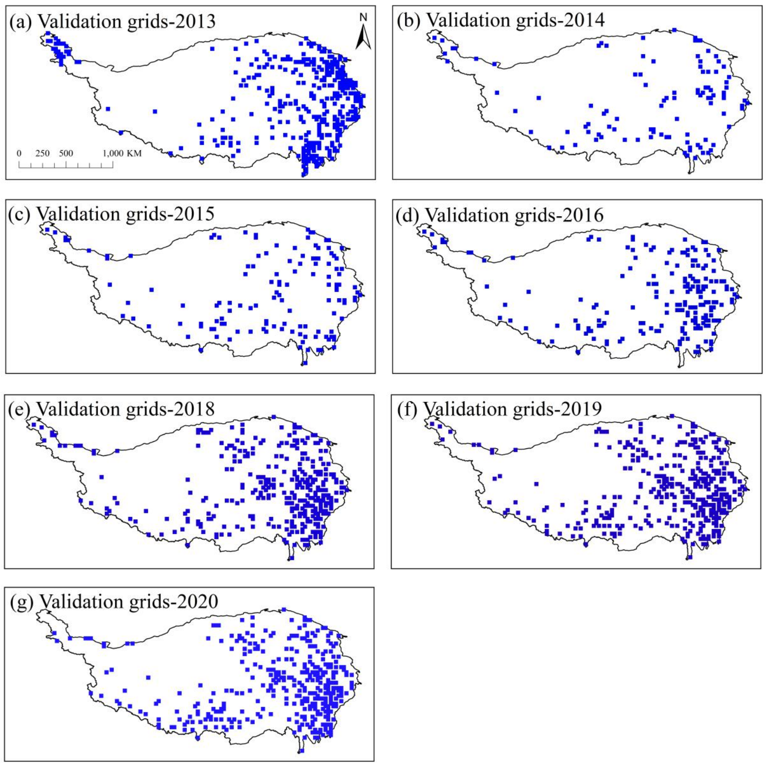

Figure 3. Spatial distribution of validation grids covering the TP for 2013–2020 (excluding 2017).

4 Results

4.1 Evaluation of rainfall erosivity estimation using ERA5 data

The accuracy of annual rainfall erosivity estimation using the ERA5 precipitation data for 2013–2020 was assessed and compared with the r_{obs_year} values in 280 grids covering the TP. The correlation coefficient of the mean annual rainfall erosivity based on the observed and ERA5 precipitation data is 0.71. For most stations, the ERA5-based values were significantly underestimated (Figure 4).

https://doi.org/10.5194/essd-2021-443
Preprint. Discussion started: 3 February 2022

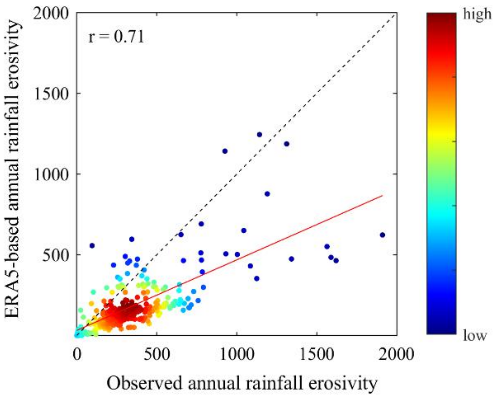

Figure 4. Comparison of mean annual rainfall erosivity based on observed and ERA5-based results for seven years (2013–2020, excluding 2017). The dotted line is the result of an optimal model (with an intercept of 0 and regression coefficient of 1). The red line is the regression result. Colors of dots represent the grid density.

To further evaluate the quality of mean annual rainfall erosivity estimation using ERA5 data, the performance of the ERA5 data in each grid was evaluated, as shown in Figure 5. The spatial pattern of the ERA5-based mean annual rainfall erosivity is consistent with that of the observed values. Specifically, areas with large annual rainfall erosivity are located mainly in the southeastern part of the plateau, especially at the southeast edge, whereas the mean annual values in the northwestern part of the plateau are relatively small. However, the observed mean annual rainfall erosivity on the TP is 344 $MJ\cdot mm\cdot ha^{-1}\cdot h^{-1}\cdot yr^{-1}$, and the ER5-based results underestimate this value by 47%. Moreover, except for most of the grids in the northwest corner and individual grids in the southeastern part of the plateau, the mean annual rainfall erosivity values in most grids in the TP are lower than the observed values.

https://doi.org/10.5194/essd-2021-443
Preprint. Discussion started: 3 February 2022

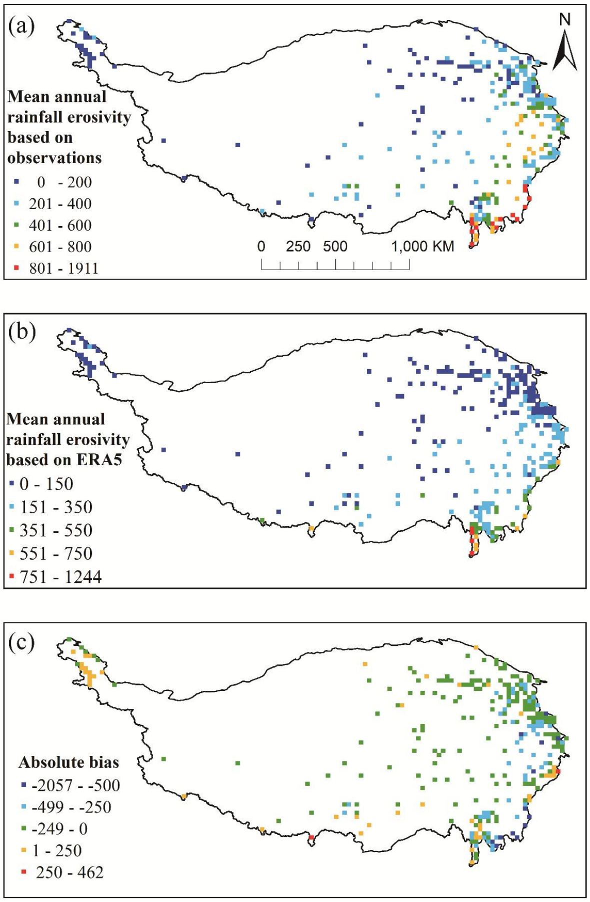

Figure 5. Mean annual rainfall erosivity in 2013–2020 (excluding 2017) based on (a) in situ precipitation observations and (b) ERA5 reanalysis precipitation data. (c) *AB* between the values based on ERA5 reanalysis data and precipitation observations.

The accuracy of the spatiotemporal variability of the mean annual rainfall erosivity on the TP obtained using the ERA5 dataset is also crucial for determining whether ERA5 is suitable for rainfall erosivity calculation. We used the first three EOF modes, which are considered to provide most of the valuable information, for evaluation. The spatial pattern of the first three EOFs of the observed values accounts for 77% of the total variance, and that of the first there EOFs of the ERA5-based values accounts for 84% of the total variance (Figure 6). Clearly, ERA5 successfully captured the spatial pattern of the EOF modes, especially the first two EOF modes, revealed by the observed values. In addition, the corresponding principal components of the EOF modes of the ERA5-based values are also consistent

https://doi.org/10.5194/essd-2021-443
Preprint. Discussion started: 3 February 2022

with the temporal variation trend of the observed values. Therefore, it can be concluded that the ERA5-based mean annual rainfall erosivity generally reproduces the spatiotemporal patterns of the rainfall erosivity on the TP.

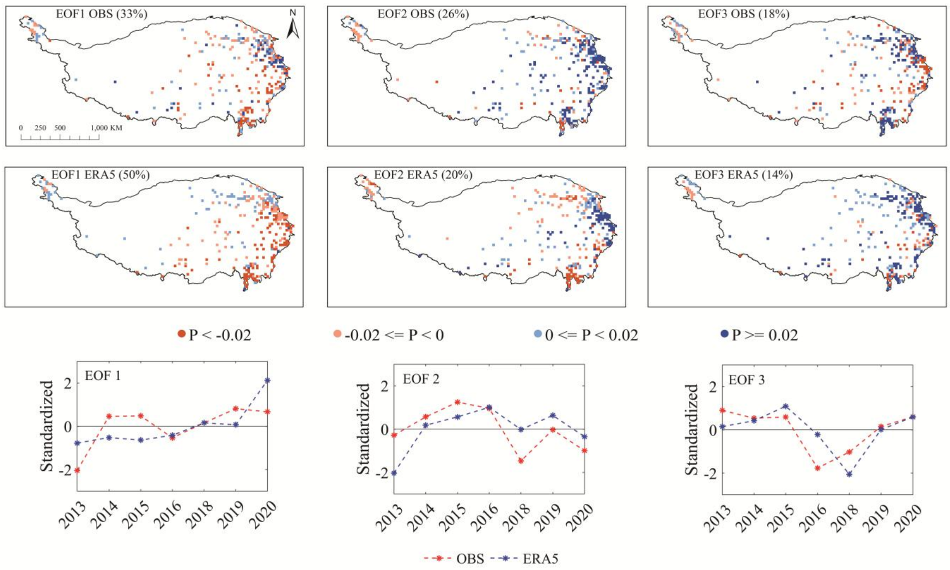

Figure 6. First three EOF modes of observed and ERA5-based mean annual rainfall erosivity on the TP in 2013–2020 (excluding 2017).

4.2 Reconstruction and validation of corrected annual rainfall erosivity

Using the observed and ERA5-based annual rainfall erosivity, we calculated the multiplier factors for 373 grids [Figure 7(a)]. The multiplier factors for the TP range from 0 to 23, with a mean value of 2.4. Multiplier factors of <1 indicate that the ERA5-based annual rainfall erosivity is overestimated, and conversely, the annual rainfall erosivity in the grid is underestimated. Most of the areas with overestimated ERA5-based mean annual rainfall erosivity are located in the Tarim, Qaidam, and Yarlung Zangpo basins. In other areas, the annual rainfall erosivity is typically underestimated, and areas with greater underestimation appear east of the Qaidam basin and in the source area of the Yellow River. We also produced a multiplier factor map of the TP by IDW interpolation based on the multiplier factors of 373 grids [Figure 7(b)].

https://doi.org/10.5194/essd-2021-443
Preprint. Discussion started: 3 February 2022

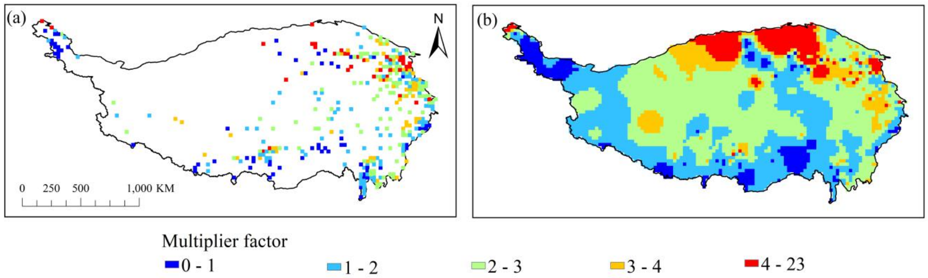

Figure 7. (a) Spatial distribution of multiplier factors of 373 grids, (b) multiplier factor map of TP generated by IDW interpolation.

The corrected annual rainfall erosivity in 2013–2020 (excluding 2017) was then calculated in the validation grids as the product of the ERA5-based annual values and multiplier factors from the map. Figure 8 compares the observed and ERA5-based annual rainfall erosivity in the validation grids by year. In 2014–2020 (excluding 2017), the multi-year averaged correction coefficient between $r_{\mathrm{obs\_year}}$ and $r_{\mathrm{cor\_year}}$ is 0.67, which is 0.13 larger than the value between $r_{\mathrm{obs\_year}}$ and $r_{\mathrm{ERA5\_year}}$. Moreover, all of the data for 2013, which were not used to produce the multiplier factor map, were used to conduct an independent assessment. The results show that the correction coefficient also increases, from 0.53 to 0.67, after the ERA5-based annual rainfall erosivity is corrected, indicating significant improvement.

https://doi.org/10.5194/essd-2021-443
Preprint. Discussion started: 3 February 2022

Open Access Earth System Science Data Discussions

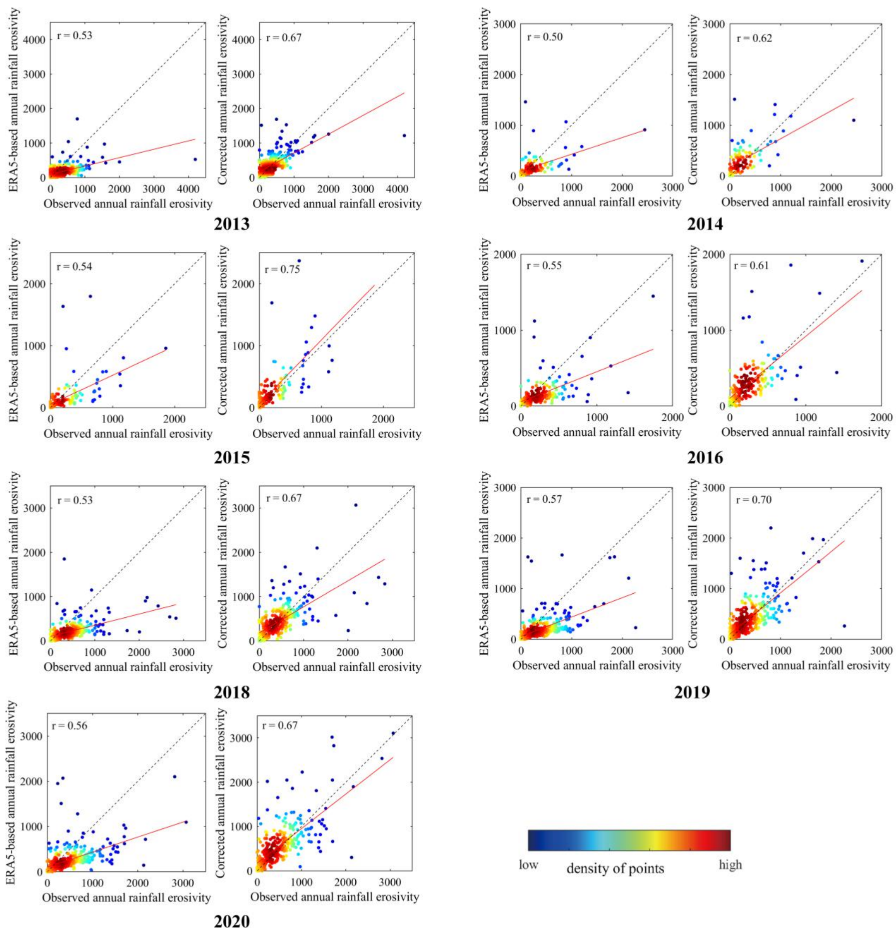

Figure 8. Comparison of ERA5-based annual rainfall erosivity (MJ·mm·ha^{-1}·h^{-1}·yr^{-1}) with observed values in validation grids for 2013–2020 (excluding 2017). The dotted line is the result of an optimal model (with an intercept of 0 and a regression coefficient of 1). The red line is the regression result. Colors of dots represent the grid density.

Violin plots are an alternative method of synthetically evaluating the accuracy of the corrected annual rainfall erosivity. Figure 9 compares the observed, ERA5-based, and corrected annual rainfall erosivity in the validation grids for 2013–2020 (excluding 2017). The corrected annual rainfall erosivity values for 2014–2020 are better than the ERA5-based values in terms of both the probability density and the values corresponding to different quantiles. Even in 2013, a completely independent verification year, the accuracy of the corrected annual rainfall erosivity is greatly improved. Specifically, the observed grid-averaged multi-year mean annual rainfall erosivity is 329 MJ·mm·ha^{-1}·h^{-1}·yr^{-1} in 2013–2020

https://doi.org/10.5194/essd-2021-443
Preprint. Discussion started: 3 February 2022

(excluding 2017), where the ERA5-based value is 190 MJ·mm·ha^{-1}·h^{-1}·yr^{-1}, and the corrected value is 374 MJ·mm·ha^{-1}·h^{-1}·yr^{-1}. The relative error is significantly reduced, from −42% to 14%, by multiplier factor correction.

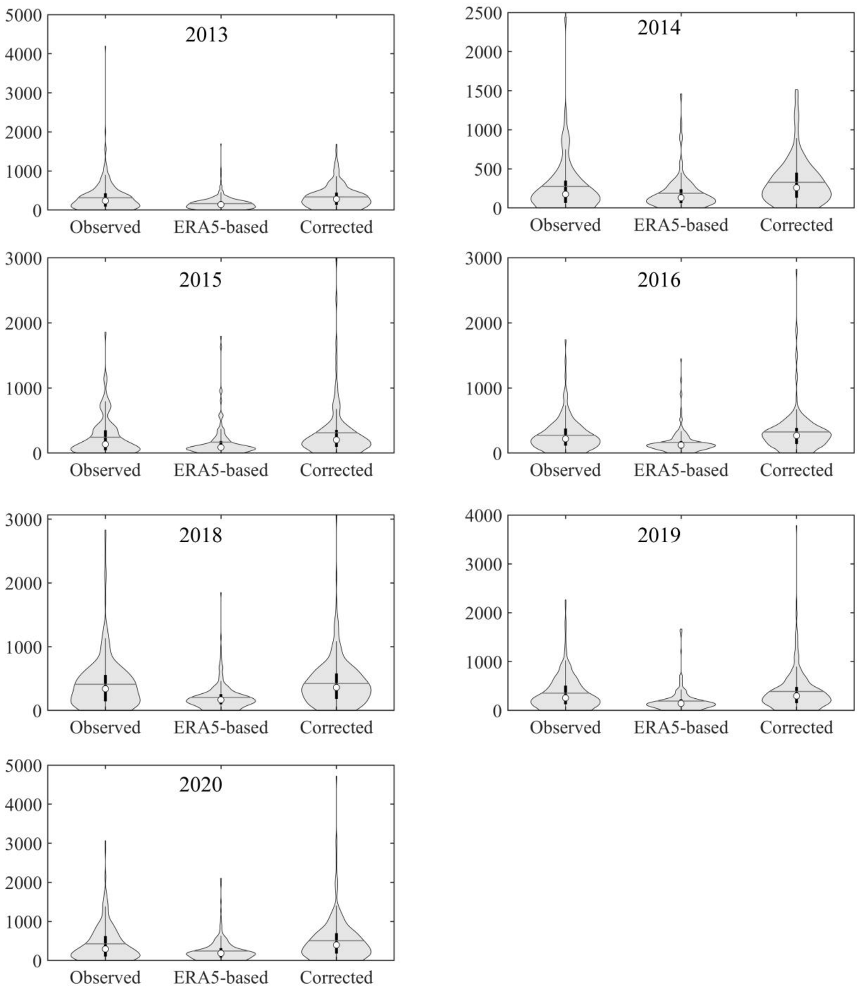

Figure 9. Violin plots of observed, ERA5-based, and corrected annual rainfall erosivity in validation grids for 2013–2020 (excluding 2017). *Y* axis shows annual rainfall erosivity in MJ·mm·ha^{-1}·h^{-1}. The boxplot diagram of the median of the violin plots shows the maximum value, 75% quantile value, 50% quantile value, 25% quantile value, and minimum value. The horizontal lines represent average values.

https://doi.org/10.5194/essd-2021-443
Preprint. Discussion started: 3 February 2022

4.3 *R* factor of TP

Because of the large variability of the spatiotemporal patterns of precipitation, the *R* factor, an essential input for soil loss estimation, must be calculated using a minimum of 20 years of precipitation data (Renard et al., 1997). In this study, the annual rainfall erosivity values of the TP for 71 years based on the 0.25° hourly ERA5 precipitation data were calculated by the algorithm shown in Section 3.1. Next, after correction by the multiplier factor map, the new annual rainfall erosivity dataset for 1950–2020 and *R* factor map were produced.

The annual rainfall erosivity fluctuates considerably within a range of 239 to 408 $MJ \cdot mm \cdot ha^{-1} \cdot h^{-1} \cdot yr^{-1}$ (Figure 10). However, no obvious increasing or decreasing trend appears in the past 71 years across the TP. Regarding the spatial distribution, the *R* factor generally shows a decreasing trend from southeast to northwest. The areas with *R* factors below 200 $MJ \cdot mm \cdot ha^{-1} \cdot h^{-1} \cdot yr^{-1}$ are concentrated in the northwestern part of the TP, whereas regions with high *R* factors appear mainly in the southeastern TP, especially in the Bomi–West Sichuan and Dawang–Chayu areas.

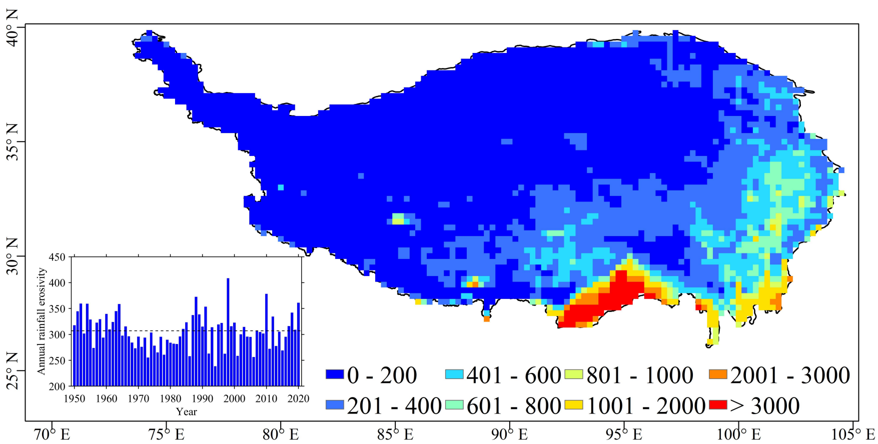

Figure 10. *R* factor map of TP with the 0.25° spatial resolution for 1950–2020. Inset represents the yearly change in annual rainfall erosivity.

When the annual rainfall erosivity across the TP is averaged, the *R* factor is 307 $MJ \cdot mm \cdot ha^{-1} \cdot h^{-1} \cdot yr^{-1}$. The *R* factor obtained in this study is clearly lower than those from previous studies, excluding that of Liu et al. (2013) (Table 2). In contrast to the published results, our study presents a data-driven approach including the use of 1-min precipitation observations from a dense network of weather

https://doi.org/10.5194/essd-2021-443
Preprint. Discussion started: 3 February 2022

stations and the 0.25° hourly ERA5 precipitation dataset to reconstruct the annual rainfall erosivity in 1950–2020.

Table 2. *R* factor of TP in previous studies

Region	Study scale	Number of weather stations	Temporal resolution	Period	*R* factor	Reference
Central and eastern TP	China	590	Daily	1960–2009	147	Liu et al., 2013
Tibet	Tibet	38	Daily	1981–2015	714	Gu et al., 2020
TP	China	756	Daily	1951–2010	408	Qin et al., 2016
Most of TP	China's dryland region	298	Daily	1961–2012	<500	Yang et al., 2015
Tibet	China	CRU_TS4	Monthly	1901–2016	3407	Cao et al., 2018
Tibet	Tibet	TRMM 3B42	Daily	2000–2008	768	Yan et al., 2010
TP	China	564	Daily	1971–1998	Cold zone: 368 Sub-cold zone: 427	Zhang et al., 2003

Note: CRU_TS4: Climatic Research Unit Time Series 4. TRMM: Tropical Rainfall Measuring Mission. Units: $MJ \cdot mm \cdot ha^{-1} \cdot h^{-1} \cdot yr^{-1}$. The boundary of the TP is identified slightly differently in these studies.

5 Data availability

The new gridded annual rainfall erosivity dataset for the TP for 1950–2020 is available at http://data.tpdc.ac.cn/en/data/37c34046-3c2a-4737-b3c9-35af398da62a/ (Chen et al., 2021).

6 Conclusions

An annual rainfall erosivity dataset for the TP for 1950–2020 was generated using station-based precipitation data from a dense network of weather stations and reanalysis data. The main conclusions are as follows:

(1) The correction coefficient between the observed mean annual rainfall erosivity on the TP and the ERA5-based values is 0.71. In addition, EOF analysis revealed that the spatiotemporal pattern of the

ERA5-based mean rainfall erosivity is consistent with that revealed by the observed values.

(2) The mean correction coefficient between the observed mean annual rainfall erosivity and the corrected values is 0.67, which is 0.13 larger than that between the observed and ERA5-based values for 2013–2020. In addition, the probability density and various quantile values of the corrected annual rainfall erosivity are also clearly improved.

(3) The area-averaged *R* factor is appropriately 307 MJ·mm·ha^{-1}·h^{-1}. The *R* factor tends to decrease from southeast to northwest. Areas with large *R* factors are concentrated mainly in the Bomi–West Sichuan and Dawang–Chayu areas.

Acknowledgments

This research was jointly supported by the Second Tibetan Plateau Scientific Expedition and Research Program (Grant No. 2019QZKK0307), the National Key R&D Program of China (Grant No. 2018YFC1507003).

Author contributions

Yueli Chen: conceptualization, methodology, and writing; Xingwu Duan: visualization, supervision, reviewing; Minghu Ding: supervision, reviewing; Wei Qi: methodology; Ting Wei: methodology; Jianduo Li: methodology.

Declaration of interests

The authors declare that they have no competing financial interests or personal relationships that could have influenced the work reported in this paper.

References

Agnese, C., Bagarello, V., Corrao, C., D Agostino, L., and D Asaro, F.: Influence of the rainfall measurement interval on the erosivity determinations in the Mediterranean area, J. Hydrol., 329(1), 39-48, doi: doi.org/10.1016/j.jhydrol.2006.02.002, 2006.

Angulo-Martínez, M., and Beguería, S.: Estimating rainfall erosivity from daily precipitation records: A

https://doi.org/10.5194/essd-2021-443
Preprint. Discussion started: 3 February 2022

comparison among methods using data from the Ebro Basin (NE Spain), J. Hydrol., 379(1), 111-121, doi: doi.org/10.1016/j.jhydrol.2009.09.051, 2009.

Brown, C.L., and Foster, R.G.: storm Erosivity Using Idealized Intensity Distributions, Trans. ASAE., 30(2), 379, doi: doi.org/10.13031/2013.31957, 1987.

Cao, Y., Wang, S.J., Bai, X.Y., and Li, H.W.: Inversion calculation and spatial-temporal pattern of rainfall erosivity in southwestern China over one hundred years, Acta Ecologica Sinica, 38(24), 8766-8773, DOI: 10.5846/stxb201805241142, 2018. In Chinese.

Chen, Y., Duan, X, Ding, M, Qi, W., Wei, T., Li, J.: 2021, A new gridded dataset of rainfall erosivity (1950-2020) in the Tibetan Plateau [dataset], National Tibetan Plateau Data Center, DOI: 10.11888/Terre.tpdc.271833, 2021.

Freitas, E.D.S., Coelho, V.H.R., Xuan, Y., Melo, D.D.C.D., Gadelha, A.N., Santos, E.A., Galvão, C.D.O., Ramos Filho, G.M., Barbosa, L.R., Huffman, G.J., Petersen, W.A., and Almeida, C.D.N.: The performance of the IMERG satellite-based product in identifying sub-daily rainfall events and their properties, J. Hydrol., 589, 125128, doi: doi.org/10.1016/j.jhydrol.2020.125128. 2020.

Gu, Z., Feng, D., Duan, X., Gong, K., Li, Y., and Yue, T.: Spatial and temporal patterns of rainfall erosivity in the Tibetan Plateau, Water, 12, 200, doi: 10.3390/w12010200, 2020.

Hersbach, H., and Coauthors, 2019: Global reanalysis: goodbye ERA-Interim, hello ERA5. doi:10.21957/vf291hehd7. https://www.ecmwf.int/node/19027.

He, J., Yang, K., Tang, W., Lu, H., Qin, J., Chen, Y., and Li, X.: The first high-resolution meteorological forcing dataset for land process studies over China, Sci. Data., 7(1), 25, doi: 10.1038/s41597-020-0369-y, 2020.

Kim, J., Han, H., Kim, B., Chen, H., and Lee, J.: Use of a high-resolution-satellite-based precipitation product in mapping continental-scale rainfall erosivity: A case study of the United States, Catena, 193, 104602, doi: doi.org/10.1016/j.catena.2020.104602, 2020.

Li, D., Yang, K., Tang, W., Li, X., Zhou, X., and Guo, D.: Characterizing precipitation in high altitudes of the western Tibetan plateau with a focus on major glacier areas, Int. J. Climatol., 40(12), 5114-5127, doi: doi.org/10.1002/joc.6509, 2020.

Liu, B., Xie, Y., Li, Z., Liang, Y., Zhang, W., Fu, S., Yin, S., Wei, X., Zhang, K., Wang, Z., Liu, Y., Zhao, Y., and Guo, Q.: The assessment of soil loss by water erosion in China, Int. Soil Water Conse., 8, doi: 10.1016/j.iswcr.2020.07.002, 2020.

https://doi.org/10.5194/essd-2021-443
Preprint. Discussion started: 3 February 2022

Liu, X., and Chen, B.: Climatic warming in the Tibetan Plateau during recent decades, Int. J. Climatol., 20(14), 1729-1742, doi: 10.1002/1097-0088(20001130)20:14<1729::AID-JOC556>3.0.CO;2-Y, 2000.

Liu, B., Tao, H., Song, C., Guo, B., Shi, Z., Zhang, C., Kong, F., and He, B.: Temporal and spatial variations of rainfall erosivity in China during 1960 to 2009, Geographical Research, 32(2): 245-256, doi: 10.11821/yj2013020005, 2013. In Chinese.

Liu, B.Y., Zhang K.L., and Xie Y., 2002. An empirical soil loss equation. In Proceedings of the 12th International Soil Conservation Organization Conference, Beijing, China, 26-31 May 2002; Tsinghua University Press: Beijing, China, 2002; Volume II, p. 15.

Lobo, G.P., and Bonilla, C.A.: Sensitivity analysis of kinetic energy-intensity relationships and maximum rainfall intensities on rainfall erosivity using a long-term precipitation dataset, J. Hydrol., 527, 788-793, doi: doi.org/10.1016/j.jhydrol.2015.05.045, 2015.

Ma, X., He, Y., Xu, J., van Noordwijk, M., and Lu, X.: Spatial and temporal variation in rainfall erosivity in a Himalayan watershed, Catena, 121, 248-259, doi: doi.org/10.1016/j.catena.2014.05.017, 2014.

Panagos, P., Borrelli, P., Meusburger, K., Yu, B., Klik, A., Jae Lim, K., Yang, J.E., Ni, J., Miao, C., Chattopadhyay, N., Sadeghi, S.H., Hazbavi, Z., Zabihi, M., Larionov, G.A., Krasnov, S.F., Gorobets, A.V., Levi, Y., Erpul, G., Birkel, C., Hoyos, N., Naipal, V., Oliveira, P.T.S., Bonilla, C.A., Meddi, M., Nel, W., Al Dashti, H., Boni, M., Diodato, N., Van Oost, K., Nearing, M., and Ballabio, C.: Global rainfall erosivity assessment based on high-temporal resolution rainfall records, Sci. REP-UK., 7(1), 4175, doi: doi.org/10.1038/s41598-017-04282-8, 2017.

Panagos, P., Meusburger, K., Ballabio, C., Borrelli, P., Beguería, S., Klik, A., Rymszewicz, A., Michaelides, S., Olsen, P., Tadić, M.P., Aalto, J., Lakatos, M., Dumitrescu, A., Rousseva, S., Montanarella, L., and Alewell, C.: Reply to the comment on “Rainfall erosivity in Europe” by Auerswald et al., Sci. Total Environ., 532, 853-857, doi: doi.org/10.1016/j.scitotenv.2015.05.020, 2015.

Qin, W., Guo, Q., Zuo, C., Shan, Z., Ma, L., and Sun, G.: Spatial distribution and temporal trends of rainfall erosivity in mainland China for 1951–2010, Catena, 147, 177-186, doi: doi.org/10.1016/j.catena.2016.07.006, 2016.

Renard, K.G., Foster, G.A., Weesies, D.K., McCool, D.K., and Yoder, D.C.: Predicting soil erosion by

https://doi.org/10.5194/essd-2021-443
Preprint. Discussion started: 3 February 2022

water: a guide to conservation planning with the revised universal soil loss equation (RUSLE). U.S. Department of Agriculture, Agriculture Handbook No. 703, 1997.

Risal, A., Lim, K.J., Bhattarai, R., Yang, J.E., Noh, H., Pathak, R., and Kim, J.: Development of web-based WERM-S module for estimating spatially distributed rainfall erosivity index (EI30) using RADAR rainfall data, Catena, 161, 37-49, doi: doi.org/10.1016/j.catena.2017.10.015, 2018.

Shin, J., Kim, T., Heo, J., and Lee, J.: Spatial and temporal variations in rainfall erosivity and erosivity density in South Korea, Catena, 176, 125-144, doi: doi.org/10.1016/j.catena.2019.01.005, 2019.

TENG, H., HU, J., ZHOU, Y., ZHOU, L., and SHI, Z.: Modelling and mapping soil erosion potential in China, J. Integr. Agr., 18(2), 251-264, doi: doi.org/10.1016/S2095-3119(18)62045-3, 2019.

Teng, H., Liang, Z., Chen, S., Liu, Y., Viscarra Rossel, R.A., Chappell, A., Yu, W., and Shi, Z.: Current and future assessments of soil erosion by water on the Tibetan Plateau based on RUSLE and CMIP5 climate models, Sci. Total Environ., 635, 673-686, doi: doi.org/10.1016/j.scitotenv.2018.04.146, 2018.

Vrieling, A., Sterk, G., and de Jong, S.M.: Satellite-based estimation of rainfall erosivity for Africa, J. Hydrol., 395(3), 235-241, doi: doi.org/10.1016/j.jhydrol.2010.10.035, 2010.

Wang, Y., Cheng, C., Xie, Y., Liu, B., Yin, S., Liu, Y., and Hao, Y. 2017. Increasing trends in rainfall-runoff erosivity in the Source Region of the Three Rivers, 1961–2012. pp. 639-648.

Wischmeier, W. H., and Smith, D. D., 1965. Predicting rainfall-erosion losses from cropland east of the Rocky Mountains: Guide for selection of practices for soil and water conservation. US 434 Department of Agriculture.

Wischmeier, W. H., and Smith, D. D., 1978. Predicting rainfall erosion losses: a guide to conservation planning. Department of Agriculture, Science and Education Administration. U. S. Department of Agriculture, Agriculture Handbook No. 537.

Xie, Y., Liu, B. Y., and Zhang, W. B.: Study on standard of erosive rainfall. Journal of Soil and Water Conservation, 14(4), 6–11, doi: 10.3321/j.issn:1009-2242.2000.04.002, 2000. In Chinese.

Yan, D., Fan, J., Guo, F., Guo, X., and Gong, K.F.: Spatiotemporal distribution of precipitation erosivity in Tibet autonomous region, Bulletin of Soil and Water Conservation, 30(3): 17-21, doi: 10.13961/j.cnki.stbctb.2010.04.025, 2010. In Chinese.

Yang, F.., and Lu, C.: Spatiotemporal variation and trends in rainfall erosivity in China's dryland region during 1961-2012, Catena, 133, 362-372, doi: dx.doi.org/10.1016/j.catena.2015.06.005, 2015. In

https://doi.org/10.5194/essd-2021-443
Preprint. Discussion started: 3 February 2022

Chinese.

Yao, T., Thompson, L., Yang, W., Yu, W., Gao, Y., Guo, X., Yang, X., Duan, K., Zhao, H., Xu, B., Pu, J., Lu, A., Xiang, Y., Kattel, D.B., and Joswiak, D.: Different glacier status with atmospheric circulations in Tibetan Plateau and surroundings, Nat. Clim. Change, 2, 663-667, doi: doi.org/10.1038/nclimate1580, 2012.

Yin, S., Xie, Y., Liu, B., and Nearing, M.: Rainfall erosivity estimation based on rainfall data collected over a range of temporal resolutions, Hydrol. Earth Syst. Sc., 19, doi: 10.5194/hess-19-4113-2015, 2015.

Yue, T., Yin, S., Xie, Y., Yu, B., and Liu, B.: Rainfall erosivity mapping over mainland China based on high density hourly rainfall records, Earth Syst. Sci. Data Discuss. Preprint, doi.org/10.5194/essd-2020-370, in review, 2021.

Zhang, W., Xie, Y., and Liu, B.: Spatial distribution of rainfall erosivity in China. Journal of Mountain Science, 21(1): 33-40, doi: 10.16089/j.cnki.1008-2786, 2003. In Chinese.